Journal of Hydrology 603 (2021) 127107

Contents lists available at ScienceDirect

Journal of Hydrology

journal homepage: www.elsevier.com/locate/jhydrol

Research papers

Stormflow generation in a humid forest watershed controlled by antecedent wetness and rainfall amounts

Guotao Zhang [a,b,c], Peng Cui [a,c,*], Carlo Gualtieri [e], Junlong Zhang [f], Nazir Ahmed Bazai [b,c,d], Zhengtao Zhang [g], Jiao Wang [b,d], Jinbo Tang [b], Rong Chen [b], Mingyu Lei [b,c]

[a] Key Laboratory of Land Surface Pattern and Simulation, Institute of Geographic Sciences and Natural Resources Research, Chinese Academy of Sciences (CAS), Beijing 100101, China
[b] Key Laboratory of Mountain Hazards and Surface Process, Institute of Mountain Hazards and Environment, CAS, Chengdu 610041, China
[c] University of Chinese Academy of Sciences, Beijing 100049, China
[d] China-Pakistan Joint Research Center on Earth Sciences, CAS-HEC, Islamabad 45320, Pakistan
[e] University of Napoli Federico II, 80125 Napoli, Italy
[f] College of Geography and Environment, Shandong Normal University, Jinan 250358, China
[g] The Key Laboratory of Environmental Change and Natural Disaster, MOE, Beijing Normal University, Beijing 100875, China

ARTICLE INFO

This manuscript was handled by Marco Borga, Editor-in-Chief, with the assistance of Yasuto Tachikawa, Associate Editor

Keywords:
Stormflow generation
Threshold behaviors
Soil water storage
Rainfall amounts
Hydrological connectivity

ABSTRACT

Understanding the meanings and identifying the controls for the stormflow generation with complex and nonlinear behaviors is essential for the development of threshold-based hydrological theory, as well as accurate assessment and prediction for flash flood risks. However, the study of catchment emergent patterns with three-linear threshold behaviors associated with hydrological connectivity has received little attention. Therefore, utilizing soil water storage, rainfall, and streamflow data spanning 3 years in a humid forest experimental watershed, Dujiangyan city, China, we elucidated how and where stormflow was generated with nonlinear behaviors, which were affected by antecedent wetness and rainfall amounts. Stormflow threshold behavior was taken as a function of combined gross precipitation and antecedent soil water storage, which was isolated using piecewise regression analysis with the identification of two breakpoints (i.e., generation threshold, T_g and rising threshold, T_r). It was found that the initial emergent behavior of rainfall-runoff was generally activated at the T_g, and then an abrupt shift from slow to fast flood response was possibly triggered at the T_r. These processes are important to understand the formation and development of flash floods at the watershed scale. It was noted that, above the T_r, considerably higher stormflow amounts generally occurred due to the lateral-connectivity extension of runoff contributing area from stream to neighboring hillslopes. Meanwhile, gravity-driven water movements in soil and better hydrological connectivity during the above-T_r phase readily triggered the huge flash flood disasters. The above-T_r flash floods with abrupt shifts were predominantly controlled by rainfall amounts, while initial below-T_g stormflow generation was mainly controlled by unsaturated soil water storage. More noteworthy, under heavy rainstorm conditions, the above-T_r stormflow was dominantly generated by subsurface flow, as was demonstrated at hillslope and watershed scales. These findings contribute to increasing our understanding of the controls on three-linear threshold-based hydrological behaviors, as well as of subsurface stormflow generation mechanism associated with hydrological connectivity in humid forest watersheds.

1. Introduction

The stormflow extremes derived by climate and anthropogenic changes become more frequent and globally damaging (Ali et al., 2015; Allan and Soden, 2008; Yin et al., 2018), and readily increase the extremes of flash floods (AghaKouchak et al., 2020; Lumbroso and Gaume, 2012). The urgency for accurate assessment and prediction for flash floods risk requires a more clear understanding of the stormflow generation mechanism and threshold behaviors in mountain headwater watersheds (Hapuarachchi et al., 2011; Ross et al., 2021).

* Corresponding author: Key Laboratory of Land Surface Pattern and Simulation, Institute of Geographic Sciences and Natural Resources Research, Chinese Academy of Sciences, Beijing 100101, China.
E-mail address: pengcui@imde.ac.cn (P. Cui).

https://doi.org/10.1016/j.jhydrol.2021.127107
Received 8 May 2021; Received in revised form 29 September 2021; Accepted 19 October 2021
Available online 26 October 2021

It was demonstrated that runoff generation mechanism in humid forest watersheds could be predominantly controlled by the limited subsurface stormflow with extremely nonlinear behaviors (Ali et al., 2013; Tromp-van Meerveld and McDonnell, 2006a; Williams et al., 2019), which remarkably differed from the reported saturation-excess overland flow (Mugabe et al., 2007) and infiltration-excess overland flow (Cammeraat, 2004; Huang et al., 2003). Tromp-van Meerveld and McDonnell (2006a) elucidated the dominant subsurface stormflow generation in a forested watershed, USA, which generally presented an emergent threshold behavior associated with hydrological connectivity and Fill-Spill theory (McDonnell et al., 2021; Tromp-van Meerveld and McDonnell, 2006b). Little or no stormflow was generated at hillslopes and contributed to the channel streamflow below the threshold for the precipitation or the sum of precipitation and soil water storage, but a significant response for the stormflow was observed once above the threshold (Detty and McGuire, 2010a; Graham et al., 2010; Tromp-van Meerveld and McDonnell, 2006a). For example, Tromp-van Meerveld and McDonnell (2006a) found an increase of 2 orders of magnitude in subsurface flow for events above the threshold compared to those events below the threshold. It well reflects the threshold behaviors for subsurface stormflow and two-linear runoff response processes, which is greatly important to get insight into the nonlinear runoff generation mechanism at hillslope and watershed scales.

Stormflow threshold behaviors were generally subject to the hydrological connectivity of the flows from hillslope to stream as the watershed runoff contributing area increased (Ali et al., 2015; Fu et al., 2013), activated by preferential flow and subsurface matrix flow (Haga et al., 2005; Tromp-van Meerveld and McDonnell, 2006a). The emergent behavior indicated a storage threshold amount but also a runoff contributing threshold area (Fu et al., 2013). Below the threshold, the runoff was generated in the near-stream zones, while the runoff contributing sources possibly extended laterally onto the upper hillslopes (Detty and McGuire, 2010a). It was noted that these behaviors could be mainly affected by rainstorm size and intensity (Buttle et al., 2019; Haga et al., 2005), antecedent soil water storage (Oswald et al., 2011; Penna et al., 2011), landscape and topography (Detty and McGuire, 2010b), soil depth and vertical hydraulic conductivity (Han et al., 2020), and forest canopy response (Scaife and Band, 2017). Larger storms could lead to more mobile water in the soil and rapid streamflow response. They possibly result in a higher value of slope derived from the storage-stormflow equation during the above-threshold phase (Fu et al., 2013). Meanwhile, high variability for stormflow amounts was often found during the above-threshold phase (Farrick and Branfireun, 2014b; Scaife and Band, 2017), mostly increasing the uncertainty in assessing and predicting the stormflow amounts affected by heavy rainstorms. It restricted our insight into the hierarchical input and output processes within the water cycle and exaggerated the uncertainty in simulating the large storms-driven flood hydrographs based on a threshold-based hydrological model. Wei et al. (2020a) proposed the stormflow generation related to three-linear threshold behaviors and demonstrated the possible co-existence of the runoff generation and rising thresholds. It could well characterize the initial streamflow activation and the transition from slow to the rapid response of stormflow, but the issue of how to efficiently elucidate the three-linear threshold behaviors is not solved (Wei et al., 2020a).

The scale issue in rainfall-runoff processes inherently exists (Ali et al., 2013). But, at the watershed scale, insights into the three-linear threshold behaviors are very essential to develop the threshold-based hydrological theory. In this study, high-resolution data (5 min) of rainfall, soil water storage, and streamflow from 2018 to 2020 were collected in a humid forest experimental watershed, southwestern China. The stormflow (i.e. quick flow) was separated from the total flow based on a two-parameter recursive digital filter method (Eckhardt, 2005), while the stormflow thresholds of combined precipitation and soil water storage for the events were identified using the piecewise regression analysis (*PRA*) method. The objectives of this work were to 1) quantitatively identify stormflow generation and rising threshold behaviors at the watershed scale, 2) exploit the dynamic controls of antecedent wetness and rainfall amounts to the three-linear threshold hydrological behaviors with the transition from slow to rapid runoff generation, and 3) gain insight into the dominant subsurface stormflow generation associated with hydrological connectivity at hillslope and watershed scales. It is very important for understanding the shift from slow to rapid runoff generation and the causes of the catastrophic flash floods associated with the strategies of prevention and mitigation in humid forest watersheds.

2. Study area

The study was conducted in the Longxi River (LXR) Experimental Watershed (31°N, 103°E), ~ 80 km northwest of Chengdu city, Sichuan Province, China (Fig. 1a and b). This watershed, as the first level tributary of the Minjiang River Basin, has a drainage area of 78.3 km^2 and a total length of 18.2 km. This region is characterized by a subtropical and humid monsoon climate with an average annual temperature of ~15.2℃. The mean annual rainfall is approximately 1135 mm with maximum precipitation occurring in August, and 80% of the annual precipitation appears in the flood season (May–October) when high-magnitude flash flood disasters probably occur (Zhang et al., 2019).

This watershed is dominated by forest land with the occupy 90.3% of the whole watershed area in 2018 (Zhang et al., 2021), mainly including *indeciduous, dark coniferous, and broad-leaf forests*. Relatively stable vegetation succession is maintained in the tenth year after the Wenchuan earthquake (Yunus et al., 2020; Zhang et al., 2021) when land development is low. The soil is classified as Haplic Luvisols, Haplic Alisols, Dystric Cambisols, and Chromic Luvisols. Soil textures mainly consist of gravel with>54%, leading to the high surface hydraulic conductivity in forest land with the values of mostly 40–200 mm/h. The bedrock type is mainly composed of granite rock (Zou et al., 2019), which is mostly with a low degree of rock weathering protected by the soils and vegetation. When the bedrock is exposed in some areas, strong weathering of the granite rock generally occurs possibly leading to a decrease of rock strength. Some bedrock depression topographies generally exist on the hillslope (Detty and McGuire, 2010b; Tromp-van Meerveld and McDonnell, 2006b), influencing the flow paths and runoff generation. Granite is characterized by poor primary permeability overall, but strong secondary permeability through cracks and fractures, if they are present, may enhance permeability. High soil surface infiltration and low granite rock percolation rates lead to a significant soil-rock interface, readily triggering the subsurface stormflow on the interface under heavy rainfall conditions.

The region with the elevation of 870–3284 m asl is steep with an average slope of $> 20°$ and the stream gradient mostly of 287–626‰. The stream channels are deeply incised with the free faces of approximately 0.3–7.0 m high. The channel width ranges from < 0.3 m in the upper reaches to 20–67 m in the middle and lower reaches. Such conditions with high relief, abundant orographic rains, and strong erosion properties (Zhang et al., 2021) readily triggered catastrophic flash floods and even debris flow events (Liu et al., 2020), such as "the 8.13 debris flow" event at the Wenchuan earthquake-affected region on August 13, 2010, with a total volume of debris materials of $\sim 7.8 \times 10^6$ m^3 (Cui et al., 2013; Xu et al., 2012).

3. Methods

3.1. Hydrometric observations

The surface flow velocity and water level automatically recorded at 5 min intervals, at gauging stations (S1–S6) distributed the whole watershed (Fig. 1c), were measured using non-contact radar Doppler flow meters (measurement accuracy: 0.01 m/s) and ultrasonic water level sensors (measurement accuracy: 0.001 m), respectively (Zhang

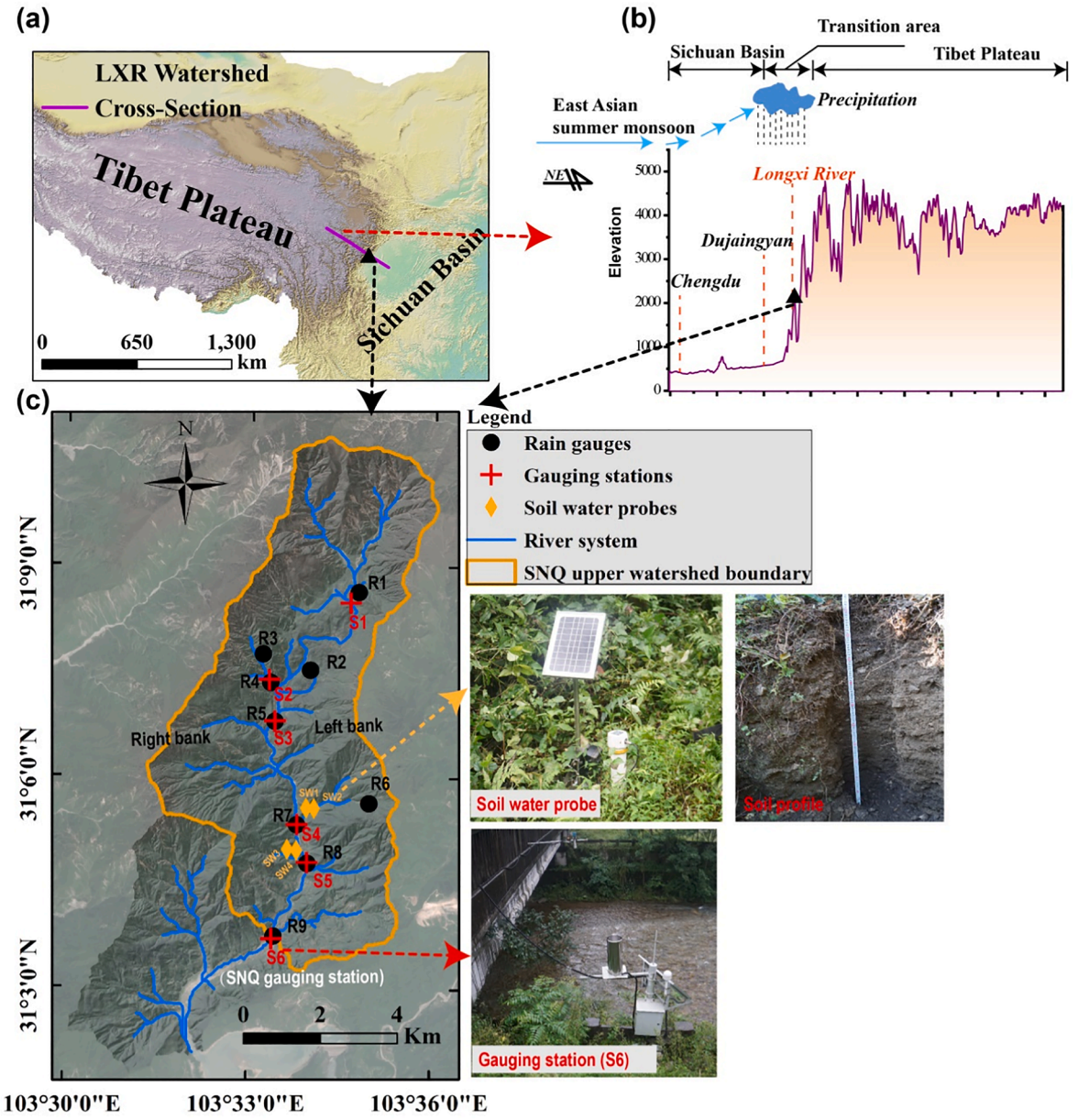

Fig. 1. Location of the Longxi River (LXR) experimental watershed in the southeastern transition area between the Sichuan Basin and the Tibet Plateau (a–b), and the detailed distributed monitoring stations and instruments (c), including six gauging stations (S1–S6), nine rain gauges (R1–R9) and four soil water probes (SW1-SW4).

et al., 2019). Six cross-sectional geometries were measured using manual surveying in combination with an unmanned aerial vehicle method. Based on the entropy and probability concepts in hydraulics (Chen, 2013; Moramarco et al., 2004), we utilized the noncontact method provided by Zhang et al. (2019) to reasonably estimate the mean cross-section velocity and flow discharge at 5 min intervals.

Field open precipitation recorded at 5 min intervals, including nine rain gauges (R1–R9) distributed into the elevations from 884 to 1834 m asl (Fig. 1c), was measured using digital tipping-bucket gauges with the resolution of 0.1 mm. Average surface rainfall in the Shuiniqiao (SNQ) upper watershed (Fig. 1c) was assessed based on the Thiessen polygon method (Zhang et al., 2021), and the collected runoff data at S6 next to the watershed outlet are analyzed and discussed (Fig. S1). Rain events were defined as a total rainfall of at least 1 mm, and individual events were separated by>6 h (Penna et al., 2011; Wei et al., 2020a). Based on the definition method for rain events, 47 events in total were identified from 2018 to 2020 in the LXR watershed. To possibly eliminate the uncertainty and nonstationary in threshold behaviors due to seasonal and inter-annual variations of land use and vegetation forest canopy (Scaife and Band, 2017), we selected the events mostly from June to August of every year from 2018 to 2020 to identify the hydrological threshold behaviors (Detty and McGuire, 2010a; Farrick and Branfireun, 2014b).

Volumetric soil moisture content (θ, cm^3 cm^{-3}) at four soil profiles (SW1-SW4) across two hillslopes was continuously measured at 5-min interval from 2018–2020 (Fig. 1c), using the Insentek Sensor Probes with temperature (±0.5℃) and soil moisture electromagnetic pulse sensors (±1 mm) (Fig. 2) provided by Insentek Technology Co., Ltd., Hangzhou, China (Qin et al., 2018). These sensors were installed in the 80 cm soil profiles below the surface at a 10 cm depth interval, powered by the equipped built-in battery and solar energy. The upper (SW1) and lower (SW2) monitored locations of one hillslope on the left bank (Fig. 1c and 2) were located in *coniferous forest land* and a mixture of *grass-shrub* land, respectively. Another monitored hillslope (SW3-SW4) on the right bank was located on the landslide. The depth equivalent antecedent soil water index (*DASI,* mm) proposed by Haga et al. (2005)

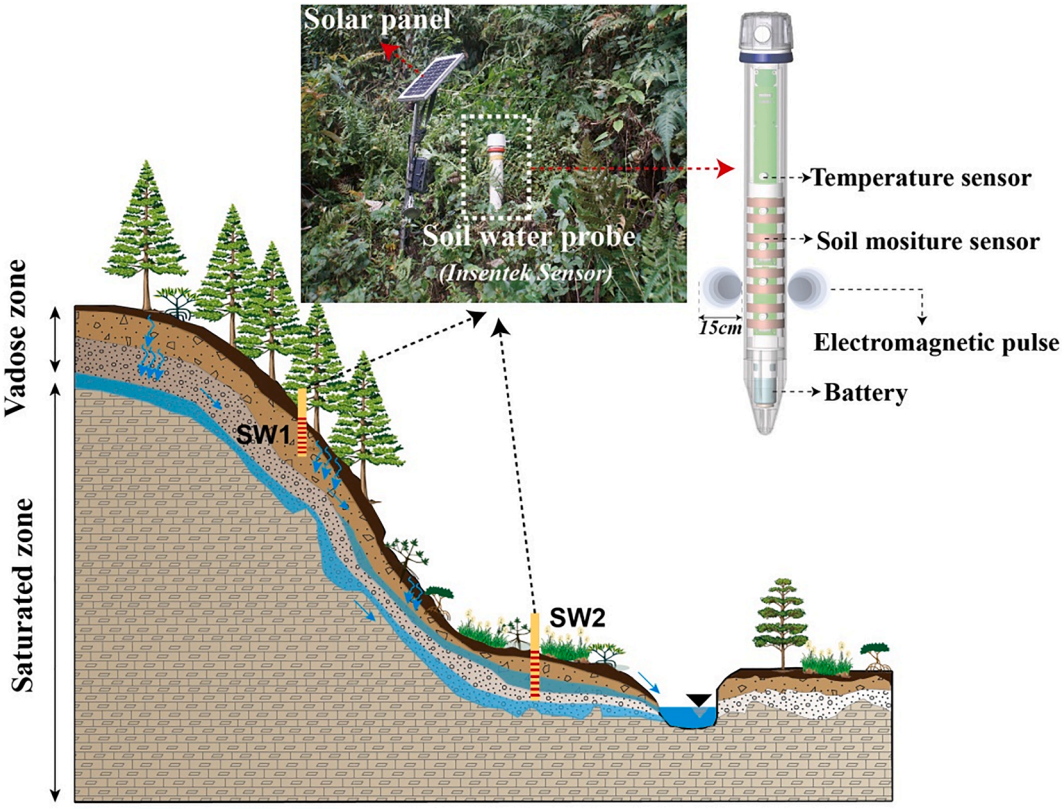

Fig. 2. Hillslope located the left bank of the watershed installed by two soil water probes (SW1-SW2, *Insentek Sensor*) equipped with temperature and soil moisture sensors.

and Wei et al. (2020a) represented the cumulative value of the initial water content at the soil profiles and elaborated the characteristics of shallow soil water storage capacity. The *DASI* at the start of each rainfall event was calculated from the eight-layer soil moisture measurements at each soil profile as (Farrick and Branfireun, 2014b; Wei et al., 2020a):

$$DASI = \sum_{i=1}^{n} \theta_i (D_i - D_{i-1}) \quad (1)$$

where θ_i indicates the average soil content between i and i-1 soil layer, $cm^3\ cm^{-3}$. $i = 1, 2, 3, 4\ldots\ldots n$, and n indicates the number of soil layers below the surface for the monitored soil depth of 80 cm. D_i indicates the soil depth at the i^{th} layer (10, 20, 30, 40, 50, 60, 70, and 80 cm, $D_0 = 0$). The index that integrated soil moisture with depth was utilized to well exploit the effects of antecedent wetness on the watershed hydrological behavior (Penna et al., 2011; Zhang et al., 2018).

3.2. Hydrograph separation

To more clearly understand how and where the stormflow was generated and identify the controls for stormflow to the formation and development of flash floods in a humid forest watershed, a two-parameter recursive digital filter method proposed by Eckhardt (2005) was utilized to separate the quick flow (i.e. stormflow, Q_q) and delayed flow (i.e. base flow, Q_b) from total discharge for the storm runoff events. The maximum base flow index (BFI_{max}) should be the suggested value of 0.8 for a perennial LXR stream with porous aquifers (Eckhardt, 2005). The storm runoff ratio (Q_q/P) is expressed by the ratio of stormflow amounts (Q_q) to grass precipitation amounts (P). The 'minimum contributing area' equivalent (*MCA*) with the parameter Q_q proposed by Dickinson and Whiteley (1970) indicated the watershed runoff minimum area contributing to the measured storm runoff.

3.3. Piecewise regression analysis

To efficiently characterize the stormflow threshold behavior of combined gross precipitation (P) and depth equivalent antecedent soil moisture index (*DASI*), a piecewise regression analysis (*PRA*) proposed by Oswald et al. (2011) and Muggeo (2003) could be utilized to quantitatively assess for threshold behavior at LXH watershed to calculate the threshold values (i.e. breakpoints) and the derived linear slope parameters. We acknowledge the existence of nonlinear and complex stormflow generation, but automatic searching and calculating the breakpoints and slope parameters using *PRA* with top-down approaches and maximum likelihood approach (Muggeo, 2003) could relatively efficiently determine the emergent hydrological behavior.

3.4. Soil hydraulic properties test

Soil hydraulic properties were quantitatively characterized by measuring saturated soil hydraulic conductivity (K_s) in soil profiles to identify the runoff generation under heavy rainstorm conditions (Farrick and Branfireun, 2014a). A constant-head permeameter test proposed by Zhang et al. (2020), suitable for measuring K_s in coarse-grained soil with rapid flow, was utilized to measure the K_s of the undisturbed soil cores based on a derivation of Darcy's law (Johnson et al., 2005; Zhang et al., 2020). 20 soil cores samples in multi-depth profiles at the upper and lower positions of the hillslope located on the left bank were obtained using the core-cutter method, and the multi-depth K_s values were measured in the laboratory to illustrate how K_s changed and storm-driven soil water moved.

4. Results

4.1. Rainfall-runoff relationships

Large storm events ($P > 10$ mm) with the 40-event dataset occupying 89% of the total were monitored and collected from 2018 to 2020 (Fig. S1). Event precipitation amounts (P) ranged from 16.4 to 263.9 mm with an average value of 68.0 mm (Fig. 3a), rainfall durations (D) ranged from 1.5 to 219 h with the mean value 23 h (Fig. 3c), and peak rainfall intensities (I_p) from 0.49 to 46.9 mm/h (Fig. 3d). The stormflow amounts (Q_q) for each event with the values from 0.24 to 193.57 mm shown in Fig. 3h were separated from the total runoff, and showed a statistically significant linear relationship with precipitation amounts (P) ($Q_q = -12 + 0.59*P$, $r^2 = 0.79$, $p < 0.01$, Fig. 4a). It was found that a quite high variability for Q_q occurred when the P exceeded 19 mm (Fig. 4a). The mean value (0.36) for Q_q/P shown in Fig. 3g and 4d was analogous to that values with 0.07–0.45 reported by some researchers from Europe and Australia (Farrick and Branfireun, 2014b; Jin et al., 2020; Marchi et al., 2009; Merz et al., 2006), and the Q_q/P could exceed 0.8 due to the integrated controls from antecedent wetness and rainstorm intensity (Smith et al., 1996; Smith et al., 2005). Weak linear relationships between Q_q and mean rainfall intensity (I_m), rainfall duration (D) were found (Fig. 4b-c). Especially, the runoff coefficient (α) appeared an abnormal phenomenon (i.e. $\alpha > 1$ shown in Fig. 5a), which mostly occurred in the range of event peak rainfall intensity (I_p) with 0–2.5 mm/h. This is mainly due to the relatively small rainfall intensity and the susceptibility to the control of shallow groundwater outflows around the river channel formed by previous rainfall events (Penna et al., 2011; Sidle et al., 2000).

Watershed lag times (L_p) from peak rainfall intensity to peak discharge ranged from 0.58 to 23.83 h (Fig. 3i) with two groups: <5 h and>10 h. The events ($N = 16$) with<5 h lag time accounted for 40% of the total events while the events ($N = 18$) with long lag time (>10 h) accounted for 45% of the total. Meanwhile, we found a significant negative power function relationship ($p < 0.05$) between I_p and lag time (L_p), and the strong variability for the lag time occurred when the I_p was lower than 15 mm/h (Fig. 5c) or the I_m was lower than 5 mm (Fig. 5d). When the peak flow was>59 $m^3\ s^{-1}$, the corresponding average lag time was 4.98 h. Meanwhile, the peak discharge with>200 $m^3\ s^{-1}$ could reduce the time to 3 h. This greatly increased the risk of catastrophic flash floods that are difficult to be prevented and mitigated.

4.2. Effects of antecedent soil moisture on stormflow

The depth equivalent antecedent soil water index (*DASI*) for 80 cm soil depth was calculated using Eq. (1) to characterize the shallow soil water storage, with the mean values of 78.93 ± 12.79 mm in forest land and a mean of 104.27 ± 8.84 mm in grass-shrub land. The statistical relationships between *DASI* and Q_q were not significant ($r^2 \leq 0.017$, $p > 0.05$) in all monitored soil points (Fig. 6a-b), indicating a little control of only antecedent soil moisture to stormflow. This is consistent with what was found in marine, humid temperate climate region (Coweta Hydrologic Laboratory) with sandy loam in North Carolina, USA (Scaife and Band, 2017), and different from that reported in a semi-arid inland climate-forest watershed with loess soil in Gansu Province, China (Jin et al., 2020). Three exceptions (i.e. 2020–08-15, 2020–08-29, and 2019–08-19) were found in Fig. 6a-b, characterized by that the lower values of *DASI* also led to the extremely high stormflow amounts. The result suggested that the observed extreme values of Q_q could be affected by other factors except for the *DASI* parameter, such as physiographic heterogeneity and precipitation input synchronism (Ali et al., 2015; Carey et al., 2010).

4.3. Stormflow generation and rising thresholds

A significant three-linear relationship ($p < 0.001$) was observed between *DASI* + P and Q_q (Fig. 6c-d) when the antecedent soil moisture was summed with the event precipitation amounts (P). The relationship, acturally, was different from the aforementioned relationship of P versus Q_q with strong variability and uncertainty under high rainfall intensities conditions (Fig. 4a). Based on piecewise regression analysis (*PRA*) combined with the Levenberg-Marquardt algorithm (LM), we could optimize and derive the three-linear threshold behaviors for *DASI* + P and Q_q relationship in the forest and grass-shrub lands ($r^2 > 0.88$, p <

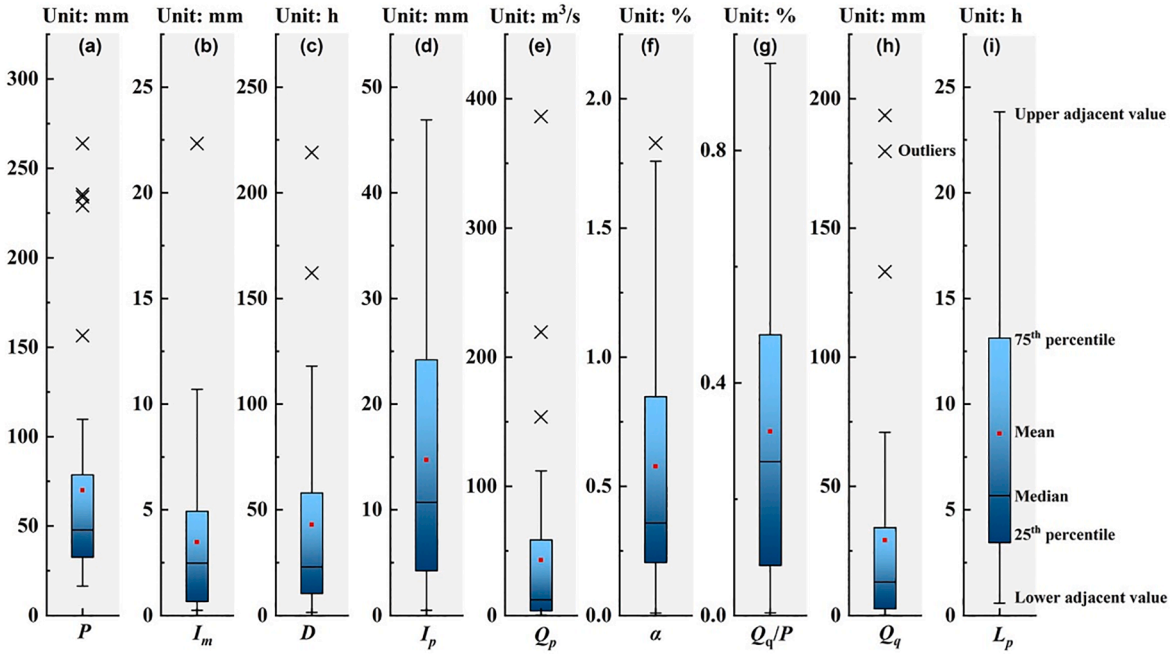

Fig. 3. Box plot of the hydrological characteristic parameters for rainfall and runoff processes. P: event precipitation amount (a), mm; I_m: mean rainfall intensity (b), mm/h; D: event rainfall duration (c), h; I_p: peak rainfall intensity (d), mm/h; Q_p: peak discharge (e), m^3/s; α: event runoff coefficient (f), %; Q_q/P: runoff ratio, % (g); Q_q: event stormflow amounts (h), mm; L_p: the watershed lag time from peak rainfall intensity to peak discharge (i), h.

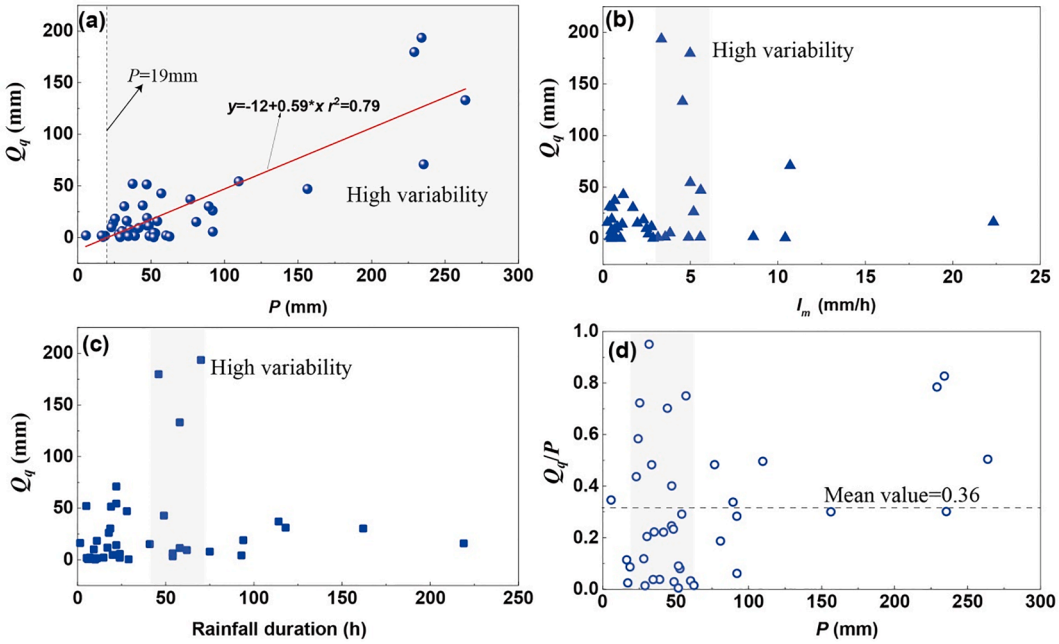

Fig. 4. Relationships between (a) event precipitation amount (P), (b) mean rainfall intensity (I_m), (c) event rainfall duration (D) and event stormflow amounts (Q_q). The relationships (d) between runoff ratio (Q_q/P) and event precipitation amount (P).

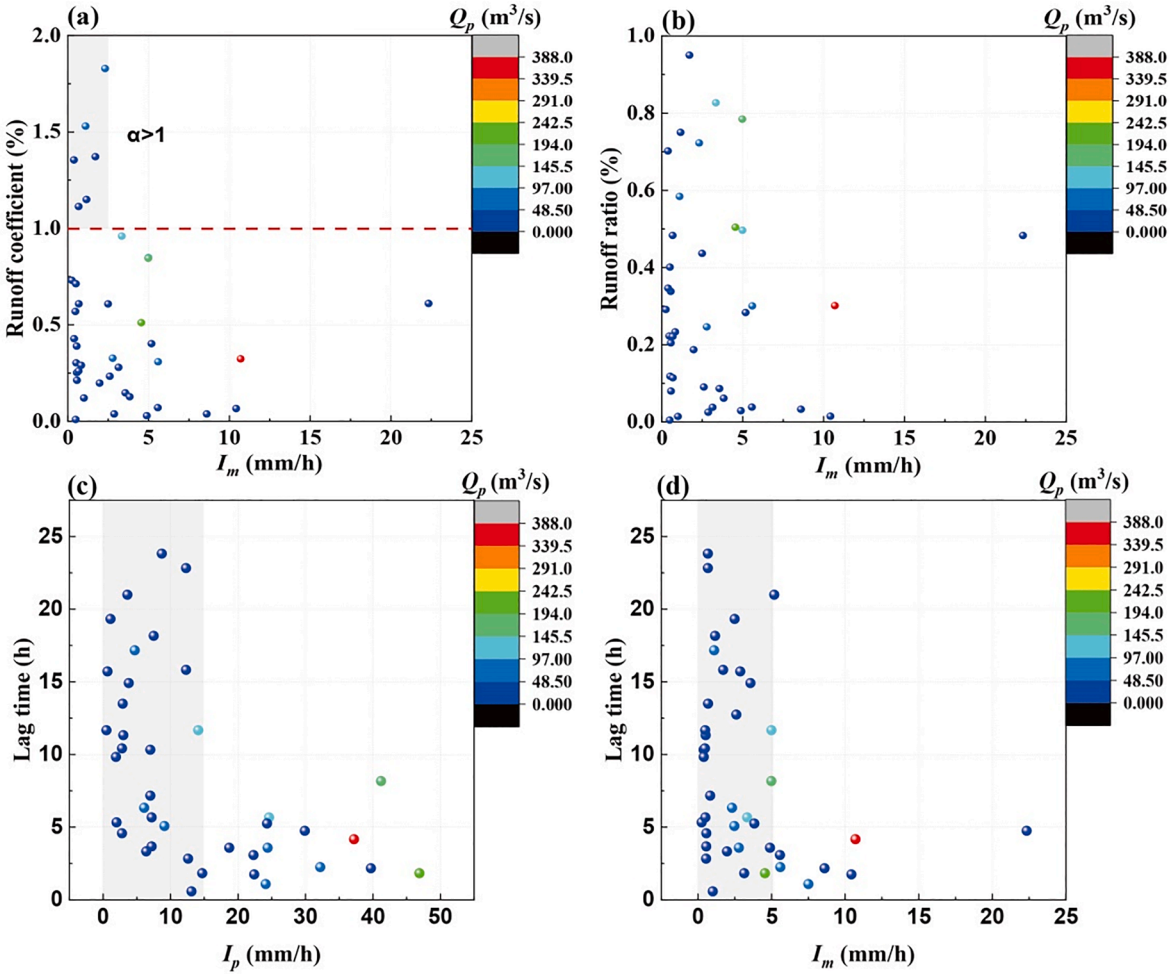

Fig. 5. Relationships between (a) event runoff coefficient (α), (b) runoff ratio (Q_q/P) and mean rainfall intensity (I_m), between lag time (L_p) and (c) peak rainfall intensity (I_p), (d) mean rainfall intensity (I_m).

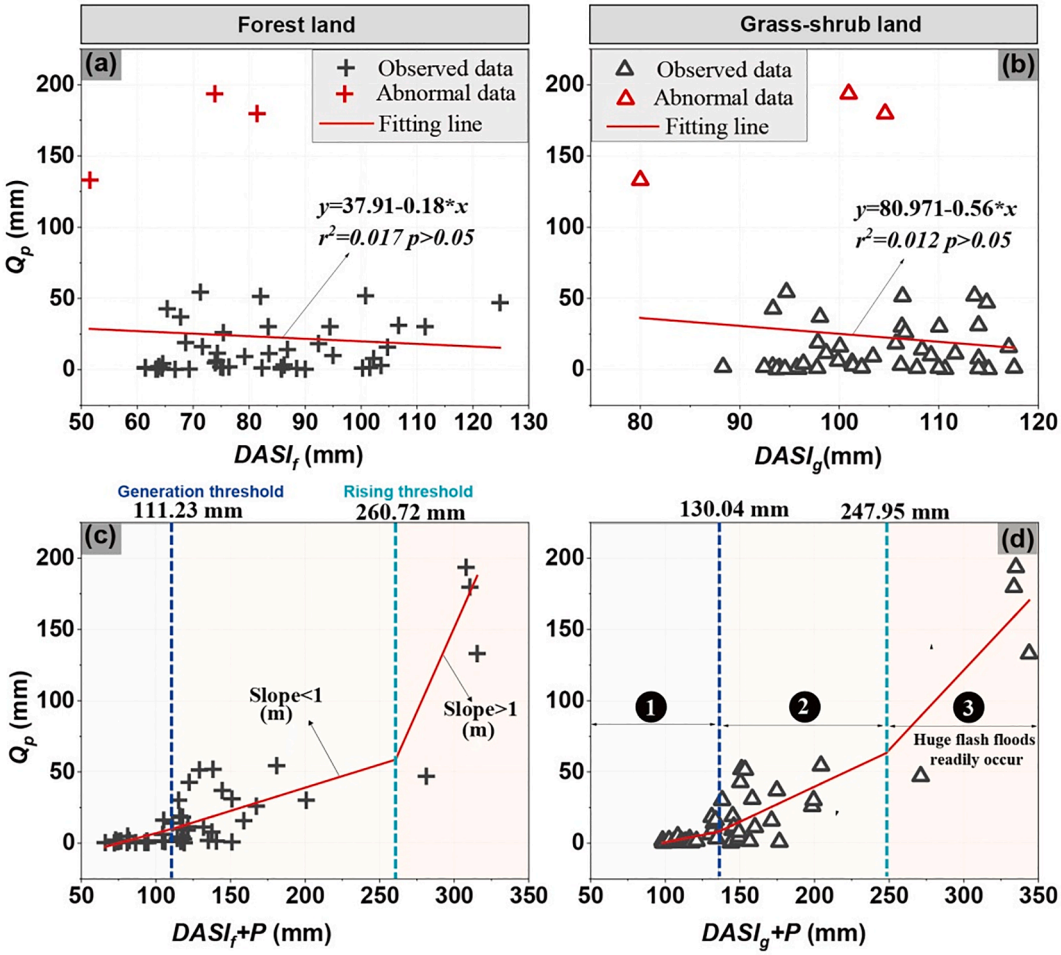

Fig. 6. Event stormflow amount (Q_q) plotted against the depth equivalent antecedent soil water index (*DASI*) at the forest (a) and grass-shrub (b) lands; Q_q plotted against the sum of event precipitation amounts (P) and *DASI* at the forest (c) and grass-shrub (d) lands. Redlines indicate the liner fitting for the variable of *DASI* and piecewise regression for the variable of $P + DASI$.

0.001, Fig. 6c-d), and obtained two thresholds (i.e. breakpoints) of each location, respectively (Table 1). The low and high thresholds were identified and demonstrated as the stormflow generation threshold (T_g) and rising threshold (T_r), respectively (Wei et al., 2020a). The lower T_g value of 111.2 mm and higher T_r value of 260.7 mm occurred in dominant forest land compared to the T_g (130.4 mm) and T_r (247.9 mm) in grass-shrub land. The initial runoff generation was mainly controlled by larger values for soil moisture deficits compared to the canopy interception capacities (Scaife and Band, 2017; Wei et al., 2020a), resulting in lower T_g value in dominant forest land. The synthesis for canopy interception capacities, soil moisture deficits, and hillslope flow pathways (Buttle et al., 2019; Ebel and Mirus, 2014; Farrick and Branfireun, 2015) can need more water input in forest land to trigger the rising threshold behaviors at the output. The generation and rising thresholds in an extremely high percentage (90.3%) for the forest land (Zhang et al., 2021) could mainly represent the hydrological threshold behaviors at the watershed scale.

Three-linear hydrological behaviors above and below the two thresholds were identified and shown in Fig. 6c-d. It was found that higher values in slope parameter ($m > 1$) of regression equations for threshold behaviors occurred in the third phasecompared to the slopes with 0.21–0.49 in the first and second phases (Table 1). It indicated the faster increase of runoff volume in the third phase when the catastrophic flash floods readily occurred. This finding of threshold-based hydrological behaviors was very important to understanding and identifying the abrupt shifts of formation and development of flash floods in a humid, steep mountain watershed.

Table 1
Parameters in assessing the threshold behaviors of $DASI + P$ and Q_q relationship at different locations based on piecewise regression analysis (PRA).

Locations	Parameters from PRA					
	r^2	T_g (mm)	T_r (mm)	m_{i1}	m_{i2}	m_{i3}
Forest land	0.88**	111.2	260.7	0.28	0.33	2.36
Grass-shrub land	0.84**	130.4	247.9	0.21	0.49	1.12

Note:
T_g indicates the generation threshold (mm).
T_r indicates the rising threshold (mm).
m_{ij} denotes the values in slope parameter of regression equations from the j_{th} phase at the i land (i = forest land and grass-shrub land, j = 1, 2, 3).
** Denotes that correlation is significant at the 0.01 level (two-tailed).

5. Discussion

5.1. Controls for hydrological threshold behaviors

It was demonstrated in the tropical dry forest or humid mountain watershed (Farrick and Branfireun, 2014b; Han et al., 2020; Zuecco et al., 2017) that when the initial soil moisture deficits for runoff generation threshold were gradually satisfied, the streamflow response can be mainly subject to the rainstorm properties. However, most studies (Ali et al., 2013; Detty and McGuire, 2010a; Fu et al., 2013; Scaife and

Band, 2017; Tromp-van Meerveld and McDonnell, 2006a; Williams et al., 2019) focused on the generation threshold behaviors with different shapes at hillslope or watershed scales, and little is considered about the integrated hydrological behaviors for runoff generation and rising thresholds (Wei et al., 2020a). Understanding how both hydrological emergent behaviors formed could help to reveal the dominant runoff producing mechanism.

Based on the analysis for the three-linear hydrological behaviors above and below the thresholds, an abrupt shift for mean Q_q with the several order of magnitudes was found during the three phases (Fig. 7e and Table 2), with values of 3.14 mm, 19.00 mm, and 138.34 mm, respectively. This shift is consistent with that reported by Oswald et al. (2011) in a small catchment in northwestern Ontario, Canada. Significantly higher values for Q_q occurred in the above-T_r phase with the large value in slope parameter ($m = 2.36$) of regression equations (Table 1), indicating the abrupt shift of flash flood above the rising threshold due to more contribution to runoff recharge from both forest canopy interception and soil water (Scaife et al., 2020; Wei et al., 2020a; Wei et al., 2020b). This is consistent with the results obtained by Scaife and Band (2017) and Buttle et al. (2019) under the condition of heavy rainstorms.

The effects of shallow soil water storage on runoff threshold behaviors are multiple and complex. Mean shallow soil storage of 19.93% at the 80 cm soil layer readily led to a significant increase in stormflow. If the shallow soil storage exceeded 24.29%, the stormflow changed more obviously with emergent behaviors. The threshold for shallow soil storage is close to the 18%–23% recorded by James and Roulet (2009) and Jin et al. (2020) but far below the 41%-46% of Western and Grayson (1998) and Penna et al. (2011). It was noted that no or little runoff was generated when the shallow soil storage is lower than the threshold of 19.93%. During the phase, the soil water flow was dominantly controlled by vertical flow movement and showed an active depth of 10–70 cm. If it was>24.29% with the emergent behavior of runoff generation in the watershed, the flow possibly generated a potential transient saturation layer below 80 cm or lateral flow at the soil–bedrock interface and formed an subsurface stormflow processes (Farrick and Branfireun, 2014b), readily resulting in an abrupt occurrence of flash flood disasters (van Meerveld et al., 2015). Additionally, the lag times (L_s) and response depths (D_s) of soil water during the three phases (Fig. 7b-c) were compared and analyzed to clearly understand the controls of soil water storage to the threshold behaviours. It was found that significantly shorter in lag time (L_s shown in Fig. 7b) for soil water response with 0.69 h occurred in the third phase below the rising threshold (Table 2). But, during the below-T_g threshold phase, the lag times (L_p shown in Fig. 7a) for runoff response were significantly shorter than that (L_s) in shallow soil water response. The soil infiltration here could be controlled by soil matric suction with hygroscopic water or film water (Jin et al., 2020), possibly resulting in slow soil water flow and long lag time (L_s) for shallow soil water. However, shorter L_s for shallow soil water with deeper response depth ($D_s > 80$ cm) was identified during the below-T_g threshold ($T_g = 111.2$ mm) phase (Fig. 7c). The hydrological behaviors below and above the two thresholds indicated the transitions from suction-driven infiltration, both capillary force and gravity-driven infiltration to only gravity-driven infiltration (Fig. 8). The proportion of freely mobile water increased once above the rising threshold in the ③ phase, readily triggering the formation and development of flash floods.

The stormflow amounts below the T_g were mainly subject to the substantially larger fraction (86.31%) of *DASI* from *DASI* + *P* shown in Fig. 7d and 8, controlled by the unsaturated soil water storage. A larger fraction (72.27%) of the *P* from *DASI* + *P* was found in the above-T_r phase (Phase ③) when the storm amounts (*P*) dominated the abrupt shift from slow to rapid flash flood generation (Fig. 8). Moreover, as in Jin et al. (2020) and Torres et al. (1998), the maximum soil moisture content (~32%) under the heavy rainstorm condition did not indicate that the soil was saturated. Therefore, the Q_q/P transition from 0.24 below the T_g to 0.60 above the T_r (Fig. 7f and Table 2) also reflected the rapid

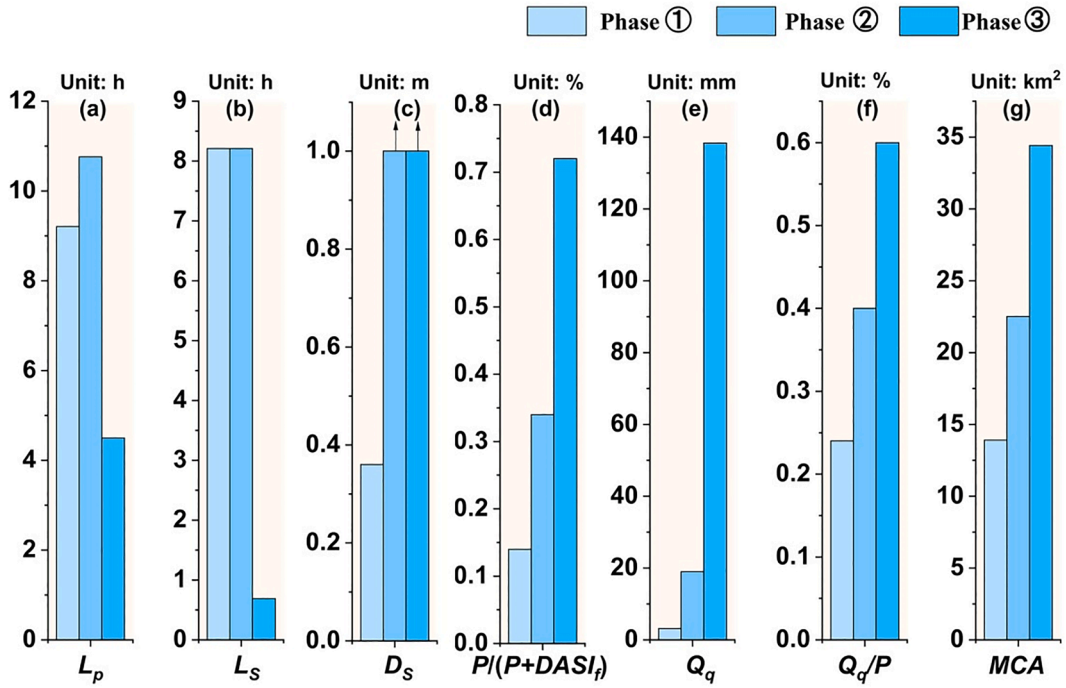

Fig. 7. The average values of each phase in hydrological parameters during three phases above and below the generation (T_g) and rising (T_r) thresholds. Phase ① is the below-T_g phase; Phase ② is the $T_g \sim T_r$ phase; Phase ③ is the above-T_r Phase. L_p: the watershed lag time from peak rainfall intensity to peak discharge (a), h. L_s: the lag time from peak rainfall intensity to peak soil moisture response at the 10–80 cm layers (b), h. D_s: the soil moisture response depth affected by rainstorms (b), m; Q_q: event stormflow amounts (d), mm. Q_q/P: the runoff ratio (e), %; $P/(P + DASI_f)$: the fraction of gross *P* from the sum between gross *P* and antecedent soil water storage in forest land (f), %. *MCA*: the runoff minimum contributing area reported by Dickinson and Whiteley (1970) (g), km^2, $MCA = Q_q/P * A$, *A* indicates the watershed area, km^2.

Table 2
The hydrological parameters in the three phases above and below the generation and rising thresholds in the Longxi River Watershed.

Phases	No.	L_p (h)	L_s (h)	D_s (m)	$P/(P + DASI_f)$ (%)	Q_q (mm)	Q_q/P (%)	MCA (km^2)
①	18	9.21	8.21	0.36	0.14	3.1	0.24	13.90
②	25	10.76	8.21	≥0.8	0.34	19.0	0.40	22.52
③	4	4.50	0.69	≥0.8	0.72	138.3	0.60	34.42

Note:
L_p: the watershed lag time from peak rainfall intensity to peak discharge, h.
L_s: the lag time from peak rainfall intensity to peak soil moisture response at 10–80 cm layers, h.
D_s: the soil moisture response depth affected by rainstorms, m.
Q_q: event stormflow amounts, mm.
Q_q/P: the runoff ratio, %.
$P/(P + DASI_f)$: the fraction of gross P from the sum between gross P and antecedent soil water storage in forest land, %.
MCA: the runoff minimum contributing area reported by Dickinson and Whiteley (1970), km^2, $MCA = Q_q/P * A$, A indicates the watershed area, km^2.

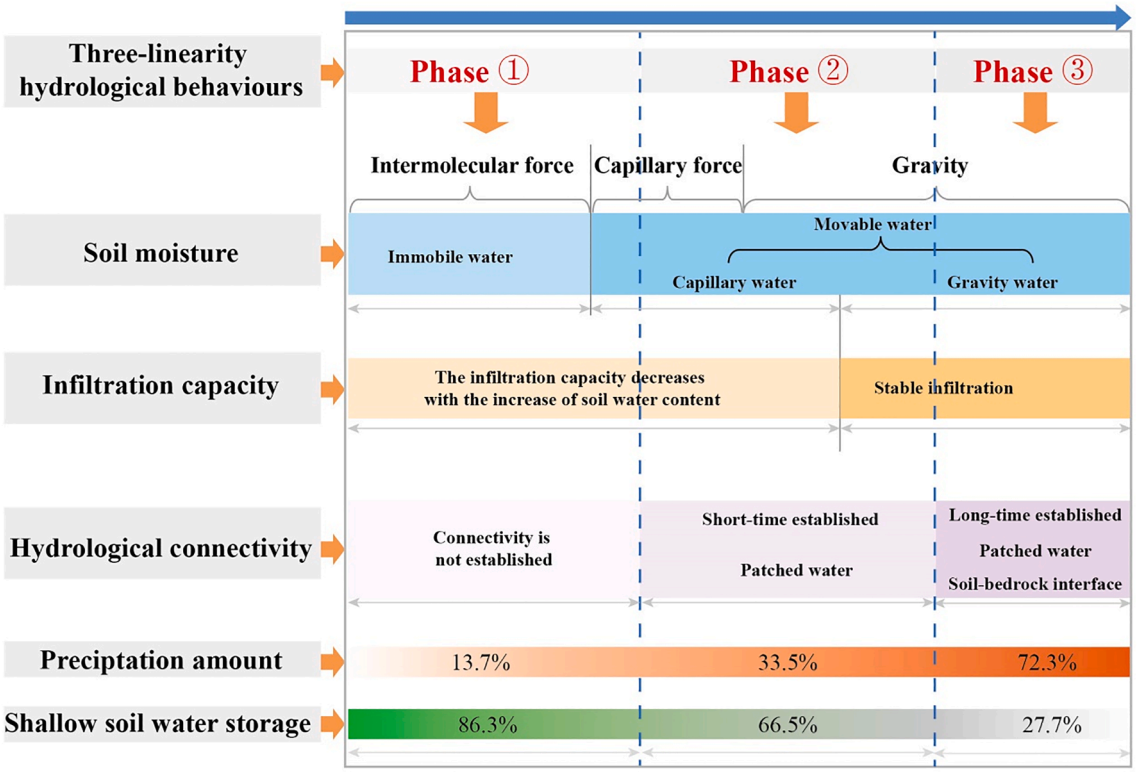

Fig. 8. Hydrological significance in soil hydrological constants and rainfall properties which controlled the three-linear hydrological behaviours.

increase of subsurface stormflow under the heavy rainstorm conditions through preferred flow pathways or soil water displacement in the unsaturated zone (McGuire and McDonnell, 2010; Torres et al., 1998). Change in the dominant factor from unsaturated soil water storage (below the T_g) to storm size and intensity (above the T_r) indicated that once the deficit for soil and canopy storage became low enough, little rainfall readily triggered more runoff translated by the storage and contributed to the formation of flash floods in a humid mountain watershed. This result is consistent with that reported by Farrick and Branfireun (2014b) in a tropical dry forest catchment, Mexico without considering the rising threshold under heavy rainstorm conditions. The extension and development for the three-linear hydrological threshold behaviors rather than two-linearity are helpful to understand the formation and development of flash floods as well as its critical abrupt shift processes induced by heavy rainstorms.

5.2. *Subsurface stormflow generation associated with hydrological connectivity*

To understand the potential subsurface stormflow generation at the hillslope scale, three representative rainfall events (2020–08-29, 2020–07-21, and 2020–08-30 shown in Fig. 9), which were below and above the generation and rising thresholds, were selected to exploit the rainfall-driven soil water movement and runoff generation associated with hydrological connectivity. For the below-T_g event (i.e., 2020-08-29 event) with precipitation amounts of 17.2 mm (Fig. 9a and d), the response time of soil water in the upper and lower hillslope was not synchronized, and the response depth is mostly within 50 cm below the surface with the small values of wetting curve maximum slope (S_{max}) (Lozano-Parra et al., 2016; Mallet et al., 2020). It indicated the soil water movement-dominated by matrix flow but little runoff, which mainly occurred in the first phase below the T_g. For the 2020–07-21 event with higher rainfall amounts of 76.6 mm between T_g and T_r (Fig. 9b and e), the response time at the 30 cm soil layer of the upper hillslope was synchronous with that at 50 cm soil layer of the lower

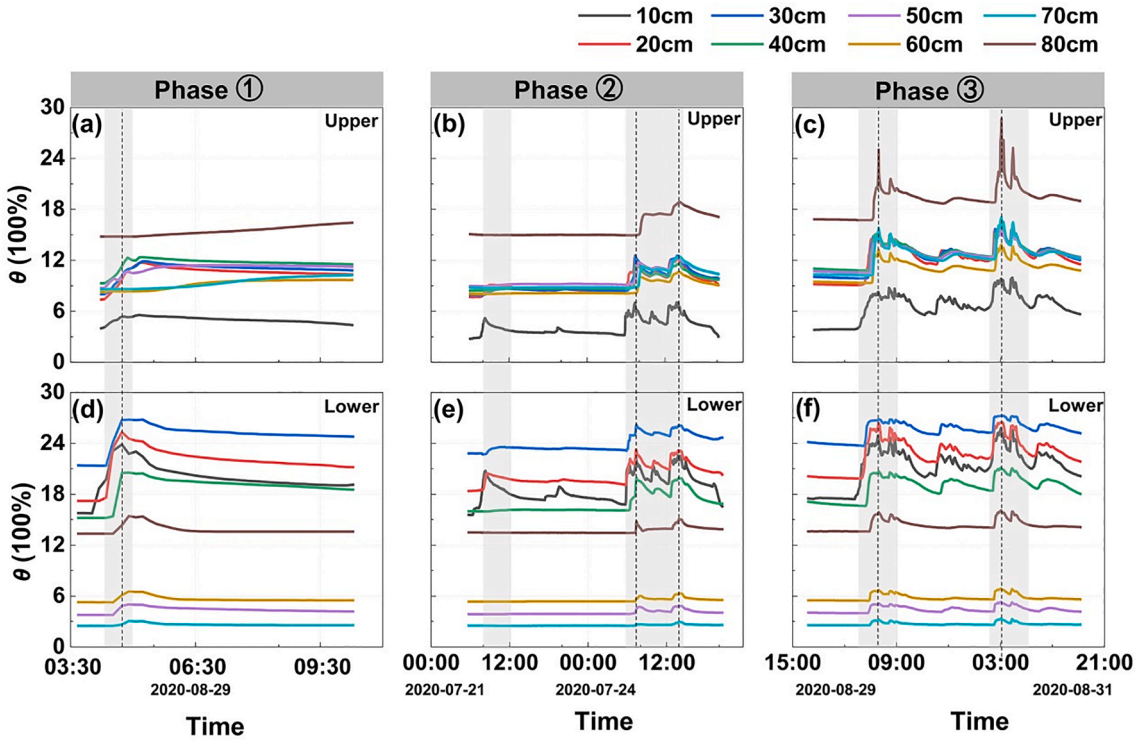

Fig. 9. Variations in monitored volumetric soil moisture content (θ) at 5-min interval for eight layers of 80 cm depth in two soil profiles at the hillslope. a, b, c denote the upper location (SW1) of the hillslope at below-T_g, $T_g \sim T_r$, above-T_r phases, respectively; d, e, f indicate the lower location (SW2) of the hillslope at below-T_g, $T_g \sim T_r$, above-T_r phases, respectively.

where the time for the instantaneous-saturation layer with perched water lasted 5–10 min. It was related to the lower saturated hydraulic conductivity measured at 30 cm layer of upper location and 50 cm layer of the lower location of the hillslope (Fig. 10). Such short connectivity time at the lower hillslope indicated the extension of the runoff contributing area from the channel nearby to the hillslope (Han et al., 2020). As storm intensity increased (2020–08-30 event with rainfall amount 229.1 mm, Fig. 9c and f), the response time of soil water in the upper and lower hillslope was synchronized with the larger S_{max}, indicating the dominant preferential flow pathways (Mallet et al., 2020). In the upper hillslope, an instantaneous saturated zone was observed at a

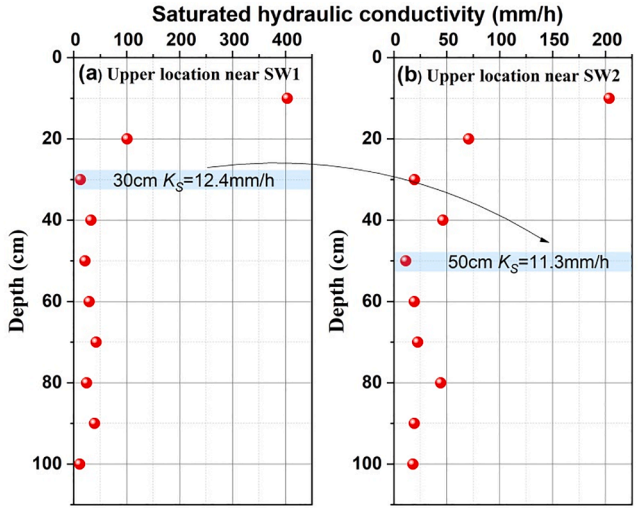

Fig. 10. Variations in saturated hydraulic conductivity with depth in two soil profiles located in the upper (a, near SW1) and lower (b, near SW2) locations of the hillslope at the left bank.

30 cm soil layer with a connectivity time of 5 min. It suggested that the contributing area, affected by a heavy rainstorm, possibly expanded laterally onto neighboring upper hillslopes (Ali et al., 2013; Detty and McGuire, 2010a; Lee and Kim, 2020), readily triggering the catastrophic flash flood disasters. This finding is important for understanding the subsurface stormflow generation mechanism associated with hydrological connectivity in a steep mountain watershed at the hillslope and watershed scales (Detty and McGuire, 2010a) and the associated shallow soil failure in slopes(Cui et al., 2014; Cui et al., 2019a; Cui et al., 2019b) and accompanied disaster chain (Guo et al., 2021; Guo et al., 2020).

At the watershed scale, the dominant stormflow generation could be identified using indirect hydrological signatures, such as the relationship between stormflow and rainfall intensity and between watershed area and lag time (Dunne, 1978; Farrick and Branfireun, 2015). At a watershed where runoff was dominated by infiltration-excess overflow (*HOF*), a significant positive linear relationship ($r^2 \geq 0.96$, $p < 0.001$) between stormflow amounts and rainfall intensity was found and verified (Cammeraat, 2004; Dunne, 1978; Martinez-Mena et al., 1998). However, in our study, the observed weak relationship between stormflow and rainfall intensity ($r^2 = 0.117$, $p = 0.484 > 0.05$) via a non-parametric test revealed that the stormflow generation was dominantly controlled by subsurface flow, demonstrating the role of subsurface streamflow in flash floods. The watershed lag time (L_p)-watershed area (A) relationship ($L_p = 0.42{*}A^{0.20}$) proposed and verified by Dunne (1978) indicated the assumption that the small experimental watershed with the size of 57 km^2 was dominantly controlled by *HOF*, where the mean lag time was calculated to be 0.94 h based on the L_p - A relationship (Fig. 11). However, the lag time in the *HOF*-dominated watershed was much shorter than that of 9.65 h observed at our experiment watershed. The result suggested that the dominant runoff generation in our experimental watershed was the subsurface stormflow, but not the *HOF*.

The relationship between stormflow and combined total precipitation and antecedent soil moisture indeed indicated the storage threshold

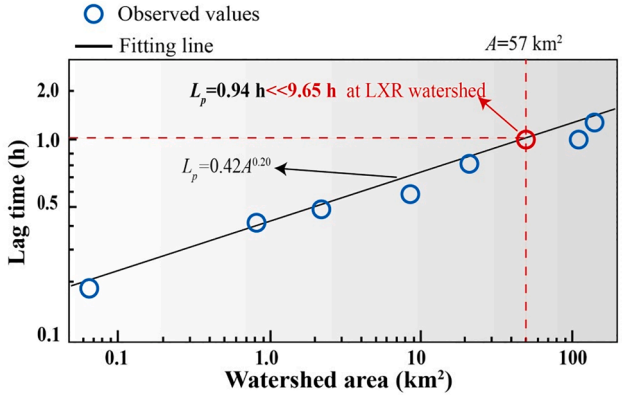

Fig. 11. Relationship between watershed lag time (L_p) and watershed area (A) at watershed where runoff was dominated by *HOF* mechanism, modified from Dunne (1978).

behaviors, but also the contributing area threshold behaviors with runoff generation (Bartlett et al., 2016; Detty and McGuire, 2010a; Kim et al., 2005; Ross et al., 2021; Scaife and Band, 2017; Zehe and Sivapalan, 2009). The significantly higher values of Q_q and Q_q/P above the T_r (Fig. 7e-f and Table 2) readily increased the hydrological connectivity of the hillslope-riparian-stream (Fig. 8), triggering the expansion of the runoff contributing area from the river channel nearby to the upper part of the hillslope. The process reflected the "percolation transition" characteristic of soil water storage at the hillslope when the Q_q increased to a certain extent with rainfall (Detty and McGuire, 2010a; Han et al., 2020; McDonnell, 2013; Tromp-van Meerveld and McDonnell, 2006a). The threshold behaviors could result in the continuous expansion of the effective connection area between the river channel and the adjacent hillslope. Once above the T_r, the Q_q increased rapidly while lag time (L_p) shortened significantly (Fig. 7e), generating the obvious emergent behaviors. The contributing area for stormflow generation in this watershed was estimated in light of the 'minimum contributing area' equivalent (*MCA*) proposed by Dickinson and Whiteley (1970). It was found that the mean *MCAs* below and above two thresholds were 13.79 km^2, 22.52 km^2, and 34.43 km^2, respectively (Fig. 7g and 12). Higher values of *MCA* above the T_r exceeded 60% of the watershed area, significantly increasing the hydrological connectivity of hillslope-riparian-stream and readily triggering the catastrophic flash flood disasters.

Therefore, a conceptual model presenting the subsurface stormflow generation mechanism associated with hydrological connectivity (Fig. 12) was developed to reveal the three-linear threshold-based hydrological behaviors under different rainfall intensity conditions. The stormflow generation processes below and above the generation and rising thresholds were represented by Fig. 12a, 12b, and 12c affected by the low, middle, and high rainfall intensities, respectively. Fig. 12a showed the stormflow generation during the below-T_g phase when soil water movement was predominantly controlled by matrix flow in the form of immobile water (Fig. 8, 9a and d, 12a). The channel discharge is mostly formed by direct rainfall or the recharge of shallow groundwater at the adjacent hillslope. As the rainfall intensity increased, soil water movement was gradually controlled by both matrix flow and preferential flow pathways (Fig. 12b). The potential perched water and 'Fill and Spill' process (Fu et al., 2013; Tromp-van Meerveld and McDonnell, 2006b) at the bedrock depression of the bedrock-soil interface could efficiently increase the hydrological connectivity of stream-adjacent hillslope and runoff minimum contributing area (*MCA*), leading to significantly higher Q_q values. Once above the T_r with high rainfall intensity (Fig. 12c), significantly higher values of *MCA* and Q_q were found, readily triggering the huge flash flood disasters (Fig. 12c). The flood flow was dominated by subsurface stormflow generation controlled by the storm size and intensity, mostly formed through the vertical preferential flow in coarse-grained soils.

5.3. Challenges for threshold-based hydrological behaviors associated with the stormflow generation

To clearly understand possible threshold-based hydrological behaviors associated with stormflow generation, we summarize some challenges that could be addressed in the future. We think this summary is helpful for a reasonable assessment of the threshold behaviors, and promote the development of a new unifying hydrological research framework based on nonlinear threshold theory (Ali et al., 2013).

5.3.1. Lack of watershed multiple processes monitoring

Field watershed experiment design generally focuses on the hydrological multiple processes, separately, which even are difficult to be quantitatively captured by our instruments or monitoring networks, such as subsurface matrix flow, preferential flow, pressure wave translation (Farrick and Branfireun, 2014b), etc. Additionally, limited spatial monitoring possibly increases the uncertainty in assessing the threshold behaviors at the watershed scale.

5.3.2. Nonstationary in threshold behaviors affected by abrupt disturbances and climate change

Climate change with hydroclimatic extremes could alter the seasonal and inter-annual stormflow thresholds and linear response with the variation of the ecosystem and vegetation forest canopy (Farrick and Branfireun, 2014b; Scaife and Band, 2017). They indicate the long-term complexity and non-stationarity in threshold behaviors with the uncertainty of the threshold values. Meanwhile, abrupt disturbance events (such as strong earthquakes, wildfire, ice, and snowstorm, etc.) could significantly destroy the landscape vegetation and even the vegetation-soil system (Bazai et al., 2021; Cui et al., 2009; Ebel and Mirus, 2014; Wei et al., 2020a; Zhang et al., 2021), rapidly impairing the original hydrological behavior at local and regional scales and further aggravating the nonstationary in threshold behavior.

5.3.3. Multi-scale assessment uncertainty for threshold behaviors

Effective multi-scale threshold metrics are difficult to be derived due to the effects of physiographic heterogeneity and precipitation input synchronism (Ali et al., 2015; Carey et al., 2010). The unified emergent behaviors at hillslope- or catchment scales could have not always proven successful (McDonnell et al., 2007), possibly resulting in different shapes of nonlinear threshold behaviors (Ali et al., 2013) and increasing the uncertainty in assessing the threshold behaviors. These limitations possibly hinder the development and generalization of the unified threshold-based hydrological theory.

6. Conclusions

In community-level field experiments, the current understanding of stormflow generation and the development of threshold-based hydrological behaviors is still limited. The study examined the relationship among shallow soil water storage, rainfall, and streamflow in the Longxi river experimental watershed, and identified a three-linear hydrological behavior with two storage breakpoints at the watershed scale, i.e. generation threshold (T_g) and rising threshold (T_r). These findings are very significant for identifying the abrupt shifts from slow to rapid runoff generation and flood response in such watersheds.

A conceptual model explaining the main subsurface stormflow associated with hydrological connectivity under different rainfall intensity conditions was developed to reveal the threshold-based hydrological behaviors at hillslope and watershed scales. Meanwhile, it was found that the dominant factors controlling the shift from slow to rapid runoff generation were from the unsaturated soil storage below the T_g to storm amounts above the T_r. The subsurface flow was identified as the main contribution to flash floods at hillslope and watershed scales.

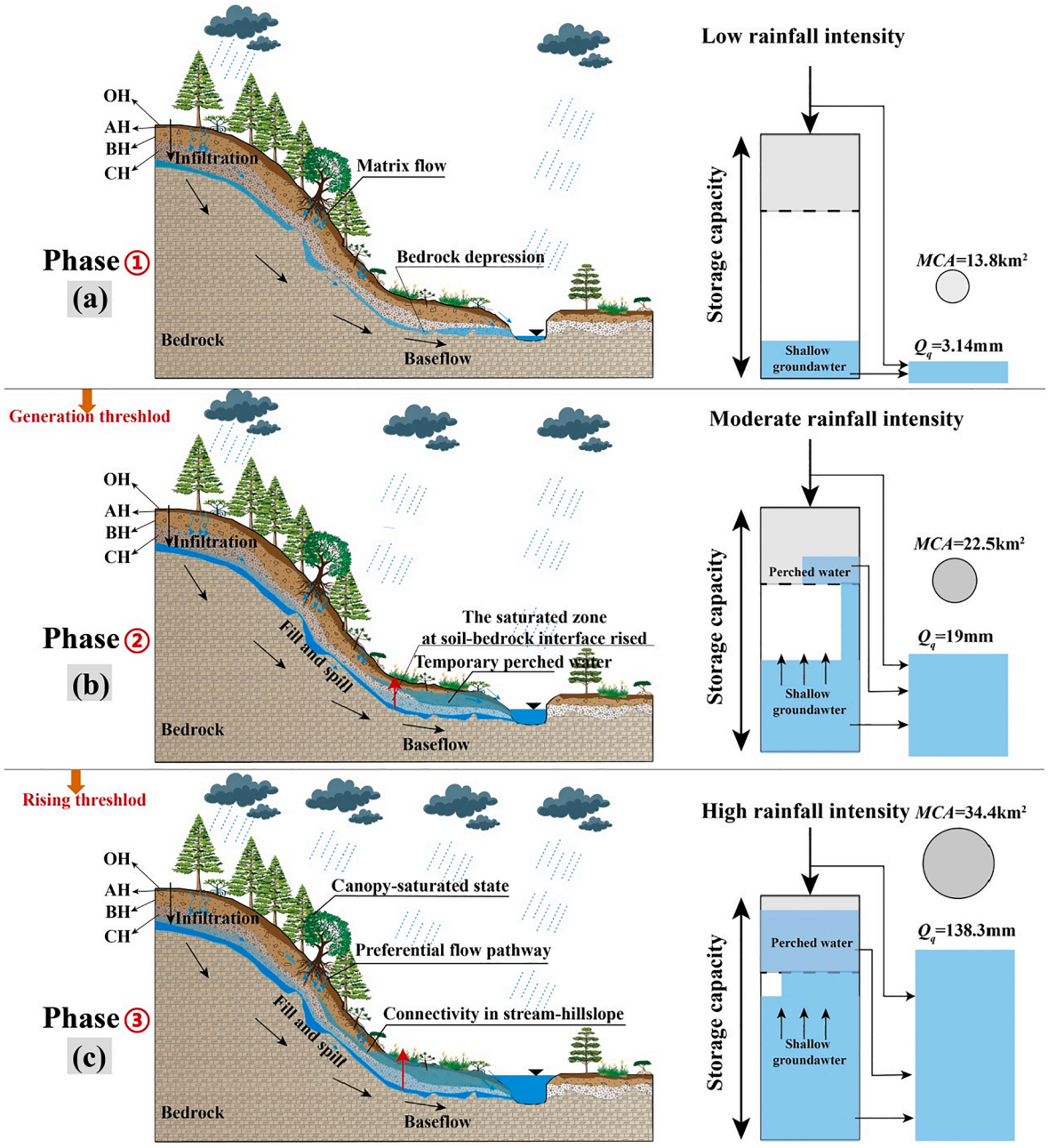

Fig. 12. A conceptual model presenting the subsurface stormflow generation mechanism associated with hydrological connectivity under different rainfall intensity conditions below and above the generation and rising thresholds.

More importantly, above the T_r, the connectivity of subsurface saturated flow lasted 5–10 min, while significantly higher values of contributing areas and stormflow amounts were found during the above-T_r phase, readily triggering huge flash flood disasters. These findings suggested that the source area possibly laterally expanded from stream onto neighboring upper hillslopes, and also highlighted the potential threshold behaviors of the contributing area associated with runoff generation.

CRediT authorship contribution statement

Guotao Zhang: Conceptualization, Methodology, Software, Data curation, Visualization. **Peng Cui:** Conceptualization, Supervision, Funding acquisition, Project administration. **Carlo Gualtieri:** Supervision, Writing – review & editing. **Junlong Zhang:** Software, Data curation. **Nazir Ahmed Bazai:** Writing – review & editing. **Zhengtao Zhang:** Supervision, Writing – review & editing. **Jiao Wang:** Writing – review & editing. **Jinbo Tang:** Formal analysis. **Rong Chen:** Visualization. **Mingyu Lei:** Investigation.

Declaration of Competing Interest

The authors declare that they have no known competing financial interests or personal relationships that could have appeared to influence the work reported in this paper.

Acknowledgments

This study was jointly supported by the National Natural Science Foundation of China (Grant No. 41790432, 41941017, and

U20A20112), and the Second Tibetan Plateau Scientific Expedition and Research Program (STEP) (Grant No. 2019QZKK0906). We acknowledge the cooperation with Mr. Zhaopeng Song from Insentek Technology Co., Ltd., Hangzhou, China about the support for the Insentek Sensor Probes, and also thank for the communications and suggestions from Dr. Kegan K Farrick from the University of the West Indies, St. Augustine. Additionally, we are very grateful to the editor (Marco Borga) and two anonymous reviewers who provided numerous comments and suggestions, resulting in an improved manuscript.

Appendix A. Supplementary data

Supplementary data to this article can be found online at https://doi.org/10.1016/j.jhydrol.2021.127107.

References

AghaKouchak, A., Chiang, F., Huning, L.S., Love, C.A., Mallakpour, I., Mazdiyasni, O., Moftakhari, H., Papalexiou, S.M., Ragno, E., Sadegh, M., 2020. Climate Extremes and Compound Hazards in a Warming World. Annu. Rev. Earth Planet. Sci. 48 (1), 519–548. https://doi.org/10.1146/earth.2020.48.issue-110.1146/annurev-earth-071719-055228.

Ali, G., Oswald, C.J., Spence, C., Cammeraat, E.L.H., McGuire, K.J., Meixner, T., Reaney, S.M., 2013. Towards a unified threshold-based hydrological theory: necessary components and recurring challenges. Hydrol. Process. 27 (2), 313–318. https://doi.org/10.1002/hyp.v27.210.1002/hyp.9560.

Ali, G., Tetzlaff, D., McDonnell, J.J., Soulsby, C., Carey, S., Laudon, H., McGuire, K., Buttle, J., Seibert, J., Shanley, J., 2015. Comparison of threshold hydrologic response across northern catchments. Hydrological Process. 29 (16), 3575–3591. https://doi.org/10.1002/hyp.10527.

Allan, R.P., Soden, B.J., 2008. Atmospheric Warming and the Amplification of Precipitation Extremes. Science 321 (5895), 1481–1484. https://doi.org/10.1126/science.1160787.

Bartlett, M.S., Parolari, A.J., McDonnell, J.J., Porporato, A., 2016. Beyond the SCS-CN method: A theoretical framework for spatially lumped rainfall-runoff response. Water Resour. Res. 52 (6), 4608–4627. https://doi.org/10.1002/wrcr.v52.610.1002/2015WR018439.

Bazai, N.A., Cui, P., Carling, P.A., Wang, H., Hassan, J., Liu, D., Zhang, G., Jin, W., 2021. Increasing glacial lake outburst flood hazard in response to surge glaciers in the Karakoram. Earth Sci. Rev. 212, 103432. https://doi.org/10.1016/j.earscirev.2020.103432.

Buttle, J.M., Webster, K.L., Hazlett, P.W., Jeffries, D.S., 2019. Quickflow response to forest harvesting and recovery in a northern hardwood forest landscape. Hydrol. Process. 33 (1), 47–65. https://doi.org/10.1002/hyp.v33.110.1002/hyp.13310.

Cammeraat, E.L.H., 2004. Scale dependent thresholds in hydrological and erosion response of a semi-arid catchment in southeast Spain. Agric. Ecosyst. Environ. 104 (2), 317–332. https://doi.org/10.1016/j.agee.2004.01.032.

Carey, S.K., Tetzlaff, D., Seibert, J., Soulsby, C., Buttle, J., Laudon, H., McDonnell, J., McGuire, K., Caissie, D., Shanley, J., Kennedy, M., Devito, K., Pomeroy, J.W., 2010. Inter-comparison of hydro-climatic regimes across northern catchments: synchronicity, resistance and resilience. Hydrol. Process. 24 (24), 3591–3602. https://doi.org/10.1002/hyp.v24:2410.1002/hyp.7880.

Chen, Y.C., 2013. Flood discharge measurement of a mountain river - Nanshih River in Taiwan. Hydrol. Earth Syst. Sci. (5), 1951–1962. https://doi.org/10.5194/hess-17-1951-2013.

Cui, P., Chen, X.-Q., Zhu, Y.-Y., Su, F.-H., Wei, F.-Q., Han, Y.-S., Liu, H.-J., Zhuang, J.-Q., 2009. The Wenchuan Earthquake (May 12, 2008), Sichuan Province, China, and resulting geohazards. Nat. Hazards 56 (1), 19–36. https://doi.org/10.1007/s11069-009-9392-1.

Cui, P., Guo, C.-X., Zhou, J.-W., Hao, M.-H., Xu, F.-G., 2014. The mechanisms behind shallow failures in slopes comprised of landslide deposits. Eng. Geol. 180, 34–44. https://doi.org/10.1016/j.enggeo.2014.04.009.

Cui, P., Zou, Q., Xiang, L.-Z., Zeng, C., 2013. Risk assessment of simultaneous debris flows in mountain townships. Prog. Phys. Geogr.: Earth Environ. 37 (4), 516–542. https://doi.org/10.1177/0309133313491445.

Cui, Y., Cheng, D., Choi, C.E., Jin, W., Lei, Y., Kargel, J.S., 2019a. The cost of rapid and haphazard urbanization: lessons learned from the Freetown landslide disaster. Landslides 16 (6), 1167–1176. https://doi.org/10.1007/s10346-019-01167-x.

Cui, Y., Jiang, Y., Guo, C., 2019b. Investigation of the initiation of shallow failure in widely graded loose soil slopes considering interstitial flow and surface runoff. Landslides 16 (4), 815–828. https://doi.org/10.1007/s10346-018-01129-9.

Detty, J.M., McGuire, K.J., 2010a. Threshold changes in storm runoff generation at a till-mantled headwater catchment. Water Resour. Res. 46 (7) https://doi.org/10.1029/2009wr008102.

Detty, J.M., McGuire, K.J., 2010b. Topographic controls on shallow groundwater dynamics: implications of hydrologic connectivity between hillslopes and riparian zones in a till mantled catchment. Hydrol. Process. 24 (16), 2222–2236. https://doi.org/10.1002/hyp.7656.

Dickinson, W., Whiteley, H., 1970. Watershed areas contributing to runoff. IAHS Publ. 96, 12–26.

Dunne, T., 1978. Field studies of hillsope flow processes. Hillslope Hydrol. 227–293.

Ebel, B.A., Mirus, B.B., 2014. Disturbance hydrology: challenges and opportunities. Hydrol. Process. 28 (19), 5140–5148. https://doi.org/10.1002/hyp.10256.

Eckhardt, K., 2005. How to construct recursive digital filters for baseflow separation. Hydrol. Process. 19 (2), 507–515. https://doi.org/10.1002/(ISSN)1099-108510.1002/hyp.v19:210.1002/hyp.5675.

Farrick, K.K., Branfireun, B.A., 2014a. Infiltration and soil water dynamics in a tropical dry forest: it may be dry but definitely not arid. Hydrol. Process. 28 (14), 4377–4387. https://doi.org/10.1002/hyp.10177.

Farrick, K.K., Branfireun, B.A., 2014b. Soil water storage, rainfall and runoff relationships in a tropical dry forest catchment. Water Resour. Res. 50 (12), 9236–9250. https://doi.org/10.1002/2014WR016045.

Farrick, K.K., Branfireun, B.A., 2015. Flowpaths, source water contributions and water residence times in a Mexican tropical dry forest catchment. J. Hydrol. 529, 854–865. https://doi.org/10.1016/j.jhydrol.2015.08.059.

Fu, C., Chen, J., Jiang, H., Dong, L., 2013. Threshold behavior in a fissured granitic catchment in southern China: 1. Analysis of field monitoring results. Water Resour. Res. 49 (5), 2519–2535. https://doi.org/10.1002/wrcr.20191.

Graham, C.B., Woods, R.A., McDonnell, J.J., 2010. Hillslope threshold response to rainfall: (1) A field based forensic approach. J. Hydrol. 393 (1–2), 65–76. https://doi.org/10.1016/j.jhydrol.2009.12.015.

Guo, J., Wang, J., Li, Y., Yi, S., 2021. Discussions on the transformation conditions of Wangcang landslide-induced debris flow. Landslides 18 (5), 1833–1843. https://doi.org/10.1007/s10346-021-01650-4.

Guo, J., Yi, S., Yin, Y., Cui, Y., Qin, M., Li, T., Wang, C., 2020. The effect of topography on landslide kinematics: a case study of the Jichang town landslide in Guizhou, China. Landslides 17 (4), 959–973. https://doi.org/10.1007/s10346-019-01339-9.

Haga, H., Matsumoto, Y., Matsutani, J., Fujita, M., Nishida, K., Sakamoto, Y., 2005. Flow paths, rainfall properties, and antecedent soil moisture controlling lags to peak discharge in a granitic unchanneled catchment. Water Resour. Res. 41 (12) https://doi.org/10.1029/2005WR004236.

Han, X., Liu, J., Srivastava, P., Mitra, S., He, R., 2020. Effects of critical zone structure on patterns of flow connectivity induced by rainstorms in a steep forested catchment. J. Hydrol. 587, 125032. https://doi.org/10.1016/j.jhydrol.2020.125032.

Hapuarachchi, H.A.P., Wang, Q.J., Pagano, T.C., 2011. A review of advances in flash flood forecasting. Hydrol. Process. 25 (18), 2771–2784. https://doi.org/10.1002/hyp.v25.1810.1002/hyp.8040.

Huang, M., Zhang, L.u., Gallichand, J., 2003. Runoff responses to afforestation in a watershed of the Loess Plateau, China. Hydrol. Process. 17 (13), 2599–2609. https://doi.org/10.1002/hyp.v17:1310.1002/hyp.1281.

James, A.L., Roulet, N.T., 2009. Antecedent moisture conditions and catchment morphology as controls on spatial patterns of runoff generation in small forest catchments. J. Hydrol. 377 (3–4), 351–366. https://doi.org/10.1016/j.jhydrol.2009.08.039.

Jin, Z., Guo, L.i., Yu, Y., Luo, D.a., Fan, B., Chu, G., 2020. Storm runoff generation in headwater catchments on the Chinese Loess Plateau after long-term vegetation rehabilitation. Sci. Total Environ. 748, 141375. https://doi.org/10.1016/j.scitotenv.2020.141375.

Johnson, D.O., Arriaga, F.J., Lowery, B., 2005. Automation of a Falling Head Permeameter for Rapid Determination of Hydraulic Conductivity of Multiple Samples. Soil Sci. Soc. Am. J. 69 (3), 828–833. https://doi.org/10.2136/sssaj2004.0014N.

Kim, H.J., Sidle, R.C., Moore, R.D., 2005. Shallow lateral flow from a forested hillslope: Influence of antecedent wetness. Catena 60 (3), 293–306. https://doi.org/10.1016/j.catena.2004.12.005.

Lee, E., Kim, S., 2020. Characterization of runoff generation in a mountainous hillslope according to multiple threshold behavior and hysteretic loop features. J. Hydrol. 590, 125534. https://doi.org/10.1016/j.jhydrol.2020.125534.

Liu, D., Cui, Y., Guo, J., Yu, Z., Chan, D., Lei, M., 2020. Investigating the effects of clay/sand content on depositional mechanisms of submarine debris flows through physical and numerical modeling. Landslides 17 (8), 1863–1880. https://doi.org/10.1007/s10346-020-01387-6.

Lozano-Parra, J., van Schaik, N.L.M.B., Schnabel, S., Gómez-Gutiérrez, Á., 2016. Soil moisture dynamics at high temporal resolution in a semiarid Mediterranean watershed with scattered tree cover. Hydrol. Process. 30 (8), 1155–1170. https://doi.org/10.1002/hyp.v30.810.1002/hyp.10694.

Lumbroso, D., Gaume, E., 2012. Reducing the uncertainty in indirect estimates of extreme flash flood discharges. J. Hydrol. 414–415, 16–30. https://doi.org/10.1016/j.jhydrol.2011.08.048.

Mallet, F., Marc, V., Douvinet, J., Rossello, P., Joly, D., Ruy, S., 2020. Assessing soil water content variation in a small mountainous catchment over different time scales and land covers using geographical variables. J. Hydrol. 591, 125593. https://doi.org/10.1016/j.jhydrol.2020.125593.

Marchi, L., Borga, M., Preciso, E., Sangati, M., Gaume, E., Bain, V., Delrieu, G., Bonnifait, L., PogacÌŒnik, N., 2009. Comprehensive post-event survey of a flash flood in Western Slovenia: observation strategy and lessons learned. Hydrol. Process. 23 (26), 3761–3770. https://doi.org/10.1002/hyp.7542.

Martinez-Mena, M., Albaladejo, J., Castillo, V.M., 1998. Factors influencing surface runoff generation in a Mediterranean semi-arid environment: Chicamo watershed, SE Spain. Hydrol. Process. 12 (5), 741–754. https://doi.org/10.1002/(sici)1099-1085(19980430)12:5<741::aid-hyp622>3.0.co;2-f.

McDonnell, J.J., 2013. Are all runoff processes the same? Hydrol. Process. 27 (26), 4103–4111. https://doi.org/10.1002/hyp.v27.2610.1002/hyp.10076.

McDonnell, J.J., Sivapalan, M., Vaché, K., Dunn, S., Grant, G., Haggerty, R., Hinz, C., Hooper, R., Kirchner, J., Roderick, M.L., Selker, J., Weiler, M., 2007. Moving beyond heterogeneity and process complexity: A new vision for watershed hydrology. Water Resour. Res. 43 (7) https://doi.org/10.1029/2006WR005467.

McDonnell, J.J., Spence, C., Karran, D.J., Ilja van Meerveld, H.J., Harman, C., 2021. Fill-and-spill: A process description of runoff generation at the scale of the beholder. Water Resour. Res. 57 (5) https://doi.org/10.1029/2020WR027514 e2020WR027514.

McGuire, K.J., McDonnell, J.J., 2010. Hydrological connectivity of hillslopes and streams: Characteristic time scales and nonlinearities. Water Resour. Res. 46 (10) https://doi.org/10.1029/2010wr009341.

Merz, R., Blöschl, G., Parajka, J., 2006. Spatio-temporal variability of event runoff coefficients. J. Hydrol. 331 (3–4), 591–604. https://doi.org/10.1016/j.jhydrol.2006.06.008.

Moramarco, T., Saltalippi, C., Singh, V.P., 2004. Estimation of Mean Velocity in Natural Channels Based on Chiu's Velocity Distribution Equation. J. Hydrol. Eng. 9 (1), 42–50. https://doi.org/10.1061/(ASCE)1084-0699(2004)9:1(42).

Mugabe, F.T., Hodnett, M., Senzanje, A., 2007. Comparative hydrological behaviour of two small catchments in semi-arid Zimbabwe. J. Arid Environ. 69 (4), 599–616. https://doi.org/10.1016/j.jaridenv.2006.11.016.

Muggeo, V.M.R., 2003. Estimating regression models with unknown break-points. Stat. Med. 22 (19), 3055–3071. https://doi.org/10.1002/(ISSN)1097-025810.1002/sim.v22:1910.1002/sim.1545.

Oswald, C.J., Richardson, M.C., Branfireun, B.A., 2011. Water storage dynamics and runoff response of a boreal Shield headwater catchment. Hydrol. Process. 25 (19), 3042–3060. https://doi.org/10.1002/hyp.8036.

Penna, D., Tromp-van Meerveld, H., Gobbi, A., Borga, M., Dalla Fontana, G., 2011. The influence of soil moisture on threshold runoff generation processes in an alpine headwater catchment. Hydrol. Earth Syst. Sci. 15 (3), 689–702. https://doi.org/10.5194/hess-15-689-2011.

Qin, A., Ning, D., Liu, Z., Sun, B., Zhao, B., Xiao, J., Duan, A., 2018. Insentek Sensor: An Alternative to Estimate Daily Crop Evapotranspiration for Maize Plants. Water 11 (1), 25. https://doi.org/10.3390/w11010025.

Ross, C.A., Ali, G.A., Spence, C., Courchesne, F., 2021. Evaluating the Ubiquity of Thresholds in Rainfall-Runoff Response Across Contrasting Environments. Water Resour. Res. 57 (1) https://doi.org/10.1029/2020wr027498.

Scaife, C.I., Band, L.E., 2017. Nonstationarity in threshold response of stormflow in southern Appalachian headwater catchments. Water Resour. Res. 53 (8), 6579–6596. https://doi.org/10.1002/2017wr020376.

Scaife, C.I., Singh, N.K., Emanuel, R.E., Miniat, C.F., Band, L.E., 2020. Non-linear quickflow response as indicators of runoff generation mechanisms. Hydrol. Process. 34 (13), 2949–2964. https://doi.org/10.1002/hyp.v34.1310.1002/hyp.13780.

Sidle, R.C., Tsuboyama, Y., Noguchi, S., Hosoda, I., Fujieda, M., Shimizu, T., 2000. Stormflow generation in steep forested headwaters: a linked hydrogeomorphic paradigm. Hydrol. Process. 14 (3), 369–385. https://doi.org/10.1002/(SICI)1099-1085(20000228)14:3<369::AID-HYP943>3.0.CO;2-P.

Smith, J.A., Baeck, M.L., Steiner, M., Miller, A.J., 1996. Catastrophic rainfall from an upslope thunderstorm in the central Appalachians: The Rapidan Storm of June 27, 1995. Water Resour. Res. 32 (10), 3099–3113. https://doi.org/10.1029/96wr02107.

Smith, J.A., Sturdevant-Rees, P., Baeck, M.L., Larsen, M.C., 2005. Tropical cyclones and the flood hydrology of Puerto Rico. Water Resour. Res. 41 (6) https://doi.org/10.1029/2004wr003530.

Torres, R., Dietrich, W.E., Montgomery, D.R., Anderson, S.P., Loague, K., 1998. Unsaturated zone processes and the hydrologic response of a steep, unchanneled catchment. Water Resour. Res. 34 (8), 1865–1879. https://doi.org/10.1029/98wr01140.

Tromp-van Meerveld, H.J., McDonnell, J.J., 2006a. Threshold relations in subsurface stormflow: 1. A 147-storm analysis of the Panola hillslope. Water Resour. Res. 42 (2), 336. https://doi.org/10.1029/2004WR003778.

Tromp-van Meerveld, H.J., McDonnell, J.J., 2006b. Threshold relations in subsurface stormflow: 2. The fill and spill hypothesis. Water Resour. Res. 42 (2) https://doi.org/10.1029/2004wr003800.

van Meerveld, H.J., Seibert, J., Peters, N.E., 2015. Hillslope-riparian-stream connectivity and flow directions at the Panola Mountain Research Watershed. Hydrol. Process. 29 (16), 3556–3574. https://doi.org/10.1002/hyp.10508.

Wei, L., Qiu, Z., Zhou, G., Kinouchi, T., Liu, Y.u., 2020a. Stormflow threshold behaviour in a subtropical mountainous headwater catchment during forest recovery period. Hydrol. Process. 34 (8), 1728–1740. https://doi.org/10.1002/hyp.v34.810.1002/hyp.13658.

Wei, L., Qiu, Z., Zhou, G., Zuecco, G., Liu, Y.u., Wu, Z., 2020b. Rainfall interception recovery in a subtropical forest damaged by the great 2008 ice and snow storm in southern China. J. Hydrol. 590, 125232. https://doi.org/10.1016/j.jhydrol.2020.125232.

Western, A.W., Grayson, R.B., 1998. The Tarrawarra Data Set: Soil moisture patterns, soil characteristics, and hydrological flux measurements. Water Resour. Res. 34 (10), 2765–2768. https://doi.org/10.1029/98wr01833.

Williams, M.R., Livingston, S.J., Heathman, G.C., McAfee, S.J., 2019. Thresholds for run-off generation in a drained closed depression. Hydrol. Process. 33 (18), 2408–2421. https://doi.org/10.1002/hyp.v33.1810.1002/hyp.13477.

Xu, Q., Zhang, S., Li, W.L., van Asch, T.W.J., 2012. The 13 August 2010 catastrophic debris flows after the 2008 Wenchuan earthquake, China. Nat. Hazards Earth Syst. Sci. 12 (1), 201–216. https://doi.org/10.5194/nhess-12-201-2012.

Yin, J., Gentine, P., Zhou, S., Sullivan, S.C., Wang, R., Zhang, Y., Guo, S., 2018. Large increase in global storm runoff extremes driven by climate and anthropogenic changes. Nat. Commun. 9 (1), 4389. https://doi.org/10.1038/s41467-018-06765-2.

Yunus, A.P., Fan, X., Tang, X., Jie, D., Xu, Q., Huang, R., 2020. Decadal vegetation succession from MODIS reveals the spatio-temporal evolution of post-seismic landsliding after the 2008 Wenchuan earthquake. Remote Sens. Environ. 236, 111476. https://doi.org/10.1016/j.rse.2019.111476.

Zehe, E., Sivapalan, M., 2009. Threshold behaviour in hydrological systems as (human) geo-ecosystems: manifestations, controls, implications. Hydrol. Earth Syst. Sci. 13 (7), 1273–1297. https://doi.org/10.5194/hess-13-1273-2009.

Zhang, G., Cui, P., Jin, W., Zhang, Z., Wang, H., Bazai, N.A., Li, Y., Liu, D., Pasuto, A., 2021. Changes in hydrological behaviours triggered by earthquake disturbance in a mountainous watershed. Sci. Total Environ. 760, 143349. https://doi.org/10.1016/j.scitotenv.2020.143349.

Zhang, G., Cui, P., Yin, Y., Liu, D., Jin, W., Wang, H., Yan, Y., Ahmed, B.N., Wang, J., 2019. Real-time monitoring and estimation of the discharge of flash floods in a steep mountain catchment. Hydrol. Process. 33 (25), 3195–3212.

Zhang, J., van Meerveld, H.J., Tripoli, R., Bruijnzeel, L.A., 2018. Runoff response and sediment yield of a landslide-affected fire-climax grassland micro-catchment (Leyte, the Philippines) before and after passage of typhoon Haiyan. J. Hydrol. 565, 524–537. https://doi.org/10.1016/j.jhydrol.2018.08.016.

Zhang, Y.i., Li, H., Abdelhady, A., Yang, J., 2020. Comparative laboratory measurement of pervious concrete permeability using constant-head and falling-head permeameter methods. Constr. Build. Mater. 263, 120614. https://doi.org/10.1016/j.conbuildmat.2020.120614.

Zou, Q., Cui, P., He, J., Lei, Y., Li, S., 2019. Regional risk assessment of debris flows in China—An HRU-based approach. Geomorphology 340, 84–102. https://doi.org/10.1016/j.geomorph.2019.04.027.

Zuecco, G., Penna, D., Borga, M., 2017. Runoff generation in mountain catchments: long-term hydrological monitoring in the Rio Vauz Catchment, Italy. Cuadernos de Investigación Geográfica 44 (2), 397. https://doi.org/10.18172/cig.vol44iss210.18172/cig.3327.